Research Article | Vol. 30, No. 1 / 3 Jan 2022 / Optics Express 1

Optics EXPRESS

Femtosecond tunable light source with variable repetition rate between 640 kHz and 41 MHz with a 130 dB temporal pulse contrast ratio

MORITZ FLOESS,[1,*] TOBIAS STEINLE,[1] ILJA GERHARDT,[2] AND HARALD GIESSEN[1]

[1] 4th Physics Institute and Research Center SCoPE, University of Stuttgart, Pfaffenwaldring 57, 70569 Stuttgart, Germany
[2] 3rd Physics Institute and Research Center SCoPE, University of Stuttgart, Pfaffenwaldring 57, 70569 Stuttgart, Germany
[*] m.floess@pi4.uni-stuttgart.de

Abstract: We demonstrate a femtosecond tunable light source with a variable pulse repetition rate based on a synchronously pumped fiber-feedback optical parametric oscillator (FFOPO) that incorporates an extended-cavity design. The repetition rate can be reduced by an acousto-optical modulator in the FFOPO pump beam. The extended FFOPO cavity supports signal oscillation down to the 64th subharmonic. The high nonlinearity of the FFOPO threshold suppresses signal output for residual pump pulses that are transmitted by the pulse picker. We characterize the temporal pulse contrast ratio of the FFOPO signal output with a second-order cross-correlation measurement. This FFOPO system enables pulse picking with extraordinarily high values up to 111 dB suppression of adjacent pulses and exhibits a temporal contrast ratio that exceeds 130 dB. It generates fs-pulses with tunable wavelength from 1415–1750 nm and 2.5–3.8 µm and variable repetition rates ranging from 640 kHz to 41 MHz.

1. Introduction

Laser pulse picking is a widely used concept to decrease the pulse repetition rate or to create bursts by selecting individual pulses from an initial pulse train with a fixed pulse repetition rate. Applications such as fluorescence lifetime imaging microscopy (FLIM) typically require repetition rates in the low MHz-range due to the lifetime of the fluorophores of up to several tens of ns [1]. Ti:sapphire lasers are usually the system of choice since they provide wavelength tunability and ultra-short pulses, both necessary for FLIM applications. However, the repetition rate of commercial systems is usually in the range of ~80 MHz. This limits the relevant observation range to a maximum of ~4 ns, considering that the temporal pulse separation should cover at least 3 lifetimes. Pulse picking enables longer lifetimes by reducing the repetition rate and therefore increases the temporal pulse separation [2]. Nonlinear microscopy modalities such as second-harmonic generation and two- or three-photon absorption fluorescence benefit from lower repetition rates as thermal damage is reduced [3,4].

Typically, the laser pulse contrast ratio of pulse pickers based on acousto- or electro-optic modulators is limited to values of the order of 100:1 for adjacent and 10^4:1 for nonadjacent pulses. However, undesired residual pulses during the off-duty cycle can excite the fluorophores partially, create a background signal, and thus deteriorate the signal-to-noise ratio. One possibility to mitigate these effects is cascading pulse pickers. This, however, comes at a cost of electronic complexity, a decrease of the overall transmission efficiency and further narrowing of the spectral operating range due to physical limitations of crystal material transparency, optical coatings, and modulation efficiency.

#439226 https://doi.org/10.1364/OE.439226
Journal © 2022 Received 6 Aug 2021; revised 30 Nov 2021; accepted 8 Dec 2021; published 20 Dec 2021

Optics EXPRESS

In the realm of high-energy laser pulses in the µJ- to the J-regime used for studying high-field physical processes in solids, an extremely high temporal contrast is required, which is beyond the performance of pulse picker devices. This is crucial to suppress coherent prepulses and thus, to avoid the formation of a preplasma, which alters the entire sample dynamics [5]. Therefore, a number of passive nonlinear temporal pulse cleaning techniques are exploited, such as saturable absorbers [6–9], second-harmonic generation (SHG) [10–12], optical parametric amplification (OPA) [13–19], cross-polarized wave generation (XPW) [20–22], nonlinear birefringence [23–25], as well as self-induced plasma shuttering [26,27]. These techniques enable measurement-limited contrast ratios of up to 10^{-12} [8], however, some of them like XPW require high-energy pulses. Typically, third-order cross-correlation is employed as temporal pulse characterization technique, as it provides temporal resolution down to the fs-timescale and a dynamic range of $\sim 10^{13}$ [28].

Here, we report on a nJ-level extended-cavity FFOPO system that does not only cover a wide output wavelength range and offers a tunable pulse repetition rate but also reaches an excellent temporal contrast ratio of 130 dB. Adjacent pulses are suppressed by 111 dB. This superior contrast ratio is achieved by modulating the FFOPO pump pulses, and its performance is determined by the threshold of optical parametric oscillation versus residual parametric fluorescence. Thus, the FFOPO enhances the contrast performance of a conventional pulse picker *by 9 orders of magnitude in an all-optical manner*, whilst offering wavelength tunability with unaltered picking performance. To the best of our knowledge this temporal pulse contrast is the highest value ever reported for any pulse picking system. This system is therefore suitable for applications such as nonlinear microscopy and FLIM, and enables access to a large fluorophore lifetime range. Furthermore, it can also be considered as front-end system for high-energy laser systems, as it would provide an extremely high laser pulse contrast ratio already at the front of the amplification chain.

2. Setup

An Yb:KGW solitary laser oscillator with 8 W of average output power, 40.95 MHz pulse repetition rate at 1032 nm center wavelength and 450 fs pulse duration [29] is used to synchronously pump a singly resonant fiber-feedback optical parametric oscillator (FFOPO), as shown in Fig. 1. A 10-mm long MgO:PPLN crystal with 9 discrete grating periods between 27.91 and 31.59 µm is used as the nonlinear medium. The FFOPO exploits a linear cavity design using a polarizing beam splitter (PBS) in combination with a quarter-waveplate (QWP) for variable output coupling [30]. Coarse wavelength tuning is performed by changing the poling period, and fine tuning is done via temperature control of the PPLN crystal and by moving one of the end mirrors to adjust the relative temporal pump-signal overlap in the crystal. The coupling efficiency of the signal into the feedback fiber is typically ~40%, i.e., the feedback losses introduced by fiber coupling amounts to $1\text{-}0.4^2 = 84\%$ (double-pass through the fiber).

First, subharmonics of the pulse repetition rate are generated by pulse picking. Therefore, an acousto-optical modulator (AOM) is placed in the pump beam path prior to the FFOPO. The AOM is driven by an arbitrary waveform generator (AWG), which is electronically synchronized to the pump laser repetition rate ensuring phase-stable operation. The AWG (Zurich Instruments, UHFAWG) applies a low-duty-cycle modulation signal such that individual pump pulses are being transmitted. Hence, the pump pulse repetition rate can be reduced by an integer fraction which in the following will be denoted by m. The AOM is operated in its 1^{st} diffraction order to ensure highest possible suppression of undesired intermediate pulses. However, the finite AOM rise and fall time leads to a leading and a trailing pulse with residual pulse energies on the order of 5% of the main pulse energy, as schematically shown in Fig. 1. These residual pulses are intrinsically suppressed by the FFOPO threshold, which therefore acts as a high-contrast filter mechanism. Later, this will be discussed in more detail. The pump laser power at the AOM input is limited to ~1.25 W at the given focal spot diameter of ~50 µm in order to avoid coating

Optics EXPRESS

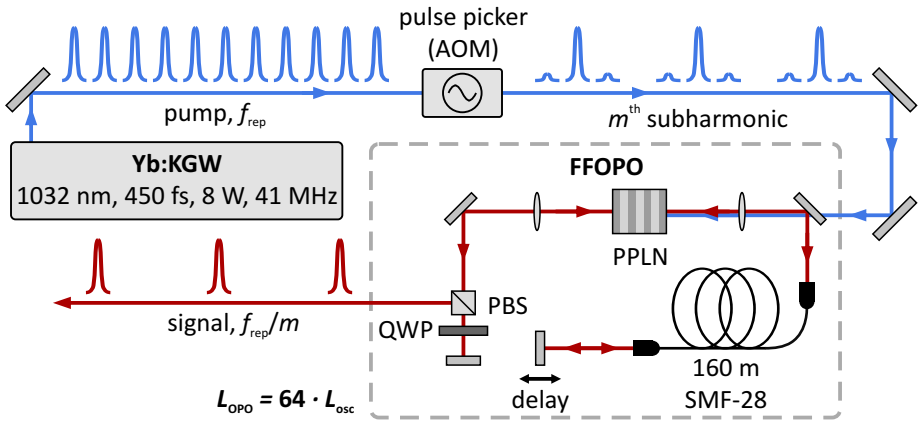

Fig. 1. Experimental setup of the FFOPO-based pulse picker. A 450-fs Yb:KGW bulk oscillator is used to synchronously pump an FFOPO based on MgO:PPLN at 1032 nm. An AOM operated in the 1st diffraction order is placed into the pump beam path to generate the m^{th} subharmonic of the fundamental repetition rate (41 MHz) by conventional pulse picking. Hereby, the leading and trailing pump pulses adjacent to the picked pulse are only suppressed by a ratio of 20:1 due to the AOM rise and fall time. The FFOPO exploits an extended cavity which incorporates a 160-m long fiber such that subharmonics up to $m = 64$ are supported. The FFOPO suppresses any pump input below the threshold pulse energy level and thus provides full modulation depth in its signal output.

damage of the AOM crystal. Thus, a pump power level of 750 mW at 41 MHz repetition rate is available at the FFOPO input. The losses are caused by the AOM diffraction efficiency of 80% at 1032 nm and subsequent optics.

As mentioned above, the FFOPO is synchronously pumped. However, rather than its cavity optical path length L_{OPO} being fundamentally matched to the optical path length L_{osc} of the pump oscillator cavity, it amounts to an integer multiple thereof, such that $L_{OPO} = N \cdot L_{osc}$. Here we choose an extended cavity with $N = 64$.

3. Results and discussion

The extended FFOPO cavity supports n independent signal cycles at the same time, where $1 \le n \le N = 64$. In the following, evenly-spaced pulse trains are being considered, meaning that the possible values for the subharmonic index m restrict the number of independent cycles in the cavity. In particular, the condition N/m being integer-valued determines the number of independent cycles. The choice $N = 64$ therefore allows the subharmonics $m = 1$, 2, 4, 8, 16, 32, and 64 being supported by the FFOPO cavity. Only at these values the signal pulses are amplified at each roundtrip.

Figure 2 demonstrates the variable signal pulse repetition rate in combination with signal wavelength tunability. Hereby, the pump pulse energy is set to 17.7 nJ, which corresponds to an average power of 725 mW at $m = 1$ (41 MHz).

Figure 2(a) exemplarily shows the signal time traces of the FFOPO operation at subharmonics $m = 1$, 2, 16, and 64, measured at a signal wavelength of 1518 nm. The time traces are recorded with an oscilloscope (Agilent Technologies, DSO9404A) at 20 GSa/s with 9 bit of vertical resolution using an InGaAs-based photodiode with 5 GHz bandwidth (Thorlabs, DET08CFC). No measurable signature of the 41 MHz fundamental frequency is left in the subharmonic traces since they are strongly suppressed by the FFOPO threshold.

Optics EXPRESS

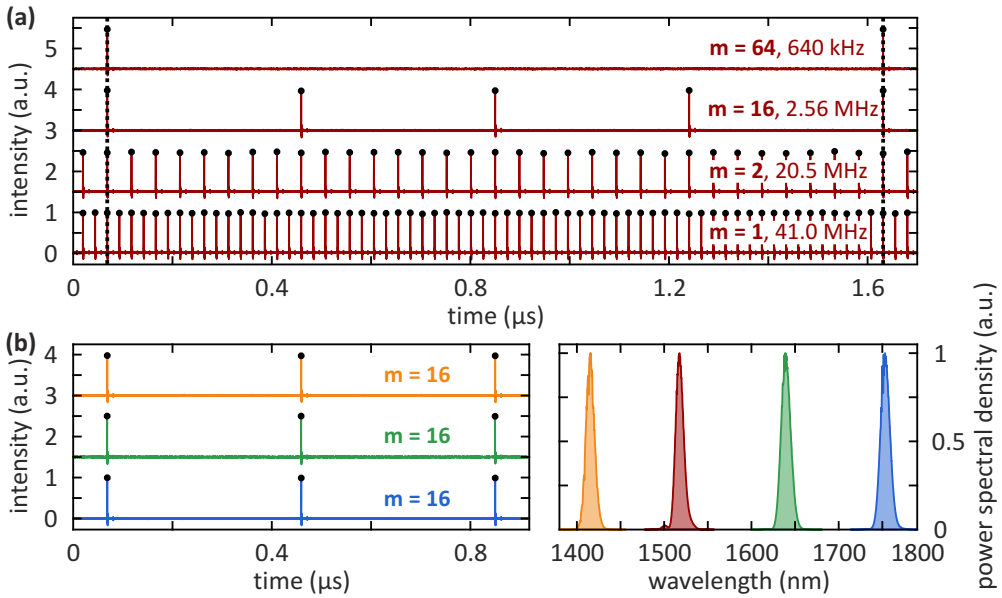

Fig. 2. **(a)** Signal output time traces at 4 different picking rates, $m = 1$, 2, 16, and 64, recorded at a fixed center wavelength of 1518 nm. The vertical dashed lines indicate the signal pulses which belong to the same cycle. At the 64th subharmonic of the pump oscillator repetition rate only one independent pulse oscillates in the FFOPO cavity. At $m = 16$ four independent pulses are launched, $m = 2$ supports 32 independent pulses, corresponding to Nyquist modulation at $f_{rep}/2$. The signal pulse repetition rate ranges from 40.95 MHz ($m = 1$) down to 640 kHz ($m = 64$). The feature trailing each signal pulse is an electronic artefact arising from impedance effects. **(b)** Wavelength tuning. Signal output time traces are measured at 1415, 1640, and 1753nm with fixed picking rate at $m = 16$. The corresponding signal spectra are shown in the right panel. The red spectrum corresponds to the data shown in **(a)**.

The vertical dashed lines indicate the signal pulses which belong to the same cycle. Thus, each of these signal pulses experience feedback from the respective previous pulse. This is the case for the 64th subharmonic of f_{rep} which marks the fundamental repetition rate of the FFOPO cavity. Thus, at $m = 64$ only a single independent signal cycle is supported. At $m = 16$ four independent cycles are launched, $m = 2$ supports 32 independent cycles, corresponding to Nyquist modulation at $f_{rep}/2$. Without pump modulation ($m = 1$) the signal output runs at f_{rep}.

Therefore, the signal pulse repetition rate ranges from 640 kHz ($m = 64$) up to 40.95 MHz ($m = 1$). Figure 2(b) demonstrates the wavelength tunability of the system. Signal output time traces are measured at 1415, 1518, 1640, and 1753 nm, where the picking rate is fixed at $m = 16$. The corresponding signal spectra are shown in the right panel. Pulse picking works over the entire tuning range of the FFOPO system without any residual leading or trailing pulses.

Due to the large amount of intra-cavity GDD a cavity length adjustment of ~50 cm is necessary to tune the signal wavelength between 1415 and 1753 nm. The measured signal bandwidth is 11–12 nm. In contrast, the calculated spectral acceptance bandwidth of the PPLN crystal is 6 nm at $\lambda_s = 1415$ nm, and 72 nm at $\lambda_s = 1753$ nm. These deviations arise from a peak-intensity dependent acceptance bandwidth and spectral filtering due to dispersion in the fiber, respectively. The latter contribution also explains the absence of strong spectral modulations in the output which might be expected from self-phase modulated feedback pulses.

Optics EXPRESS

The corresponding pulse durations fall in the range between 320 and 400 fs. This suggests that the output pulse duration is close to the Fourier limit assuming a time-bandwidth product of 0.441 (Gaussian temporal profile). Reference [31] reports signal pulse durations between 250 and 400 fs for this FFOPO system using the *fundamental* cavity configuration. An auto-correlation trace is exemplarily shown in Fig. 4(e) which will be discussed below.

The idler channel extends the tunability even further towards the mid-IR region (2509–3813 nm) with identical repetition rate and the superior contrast ratio. This is due to the inherent presence of an idler photon for each generated signal photon.

The timing jitter of the signal pulses depends on both the timing jitter of the pump oscillator and the FFOPO resonator. Passively mode-locked solid-state oscillators typically exhibit integrated RMS timing jitters of a few femtoseconds and well below. The FFOPO is optically synchronized and must therefore show similar performance. Otherwise the temporal mismatch between pump and seed pulse would induce significant relative intensity noise, which is not the case [30]. The signal pulse energy stability is measured across 2000 consecutive pulses for 725 mW of pump power and amounts to ~1.5% rms for both, the extended ($m = 1$) and the fundamental cavity configuration. Thus, the extended cavity design has no detrimental effect on the pulse energy stability.

Thermal expansion of the 160-m long feedback fiber causes an effective change of the cavity length and thus, a wavelength change. Thermal stabilization of the fiber could be implemented to prevent long-term wavelength drifts.

The extended cavity configuration does not alter the Gaussian-shaped beam profiles of signal and idler compared to fundamental cavity operation, since only the propagation length in the single-mode fiber is increased, whereas the free-space part of the cavity remains unchanged.

So far, only evenly spaced pulse trains have been considered. However, arbitrary signal pulse sequences can also be produced, e.g., bursts consisting of a few single pulses. This works if the burst periodicity corresponds to $N = 64$ pump cycles, i.e., steady-state operation is given. Furthermore, arbitrary N-values can be chosen in order to access any specific subharmonic of f_{rep}.

We now focus our investigation on the modulation contrast ratio by analyzing the threshold and energy filter behavior of the FFOPO. Figure 3(a) depicts the signal output pulse energy depending on the pump pulse energy in the range between 9.6 and 15.6 nJ. Below a pump level of 12.8 nJ no signal output occurs apart from parametric fluorescence. Hereby, the output coupling ratio is set to 75%. Figure 3(b–e) demonstrate the pulse suppression behavior in the output time trace by reducing the pump pulse energy in a controlled manner. Therefore, pump and signal time traces are shown for three different pump pulse energies as indicated in Fig. 3(a). The AOM generates a subharmonic at $m = 8$ (5.1 MHz), such that the picked pulses are separated by several AOM rise time constants (~15 ns). Additionally, every 2$^{\mathrm{nd}}$ pump pulse is partially attenuated such that the pulse suppression behavior due to the OPO threshold can be investigated, while the unattenuated pulse train serves as reference. As a guide to the eye the corresponding signal pulses are alternatingly shown in red (reference) and green (attenuated) to indicate their relationship to the modulated pump pulse train. Without attenuation (15.6 nJ, panel (b)) a steady state signal output at $m = 8$ is observed. Reducing the pulse energy to slightly above the threshold (13.0 nJ, panel (c)) leads to four individual signal cycles with different pulse energies, each corresponding to $m = 64$. Below the threshold at 12.8 nJ (panel (d)) no signal output occurs. The zoom-in (panel (e)) depicts the region between two subsequently detected signal pulses recorded at high resolution. This confirms that the signal output is suppressed for pump levels below the threshold.

So far, the characterization of the suppression of the signal output at intermediate pulse sites was based on the measurement using a photodiode and an oscilloscope. This method clearly lacks sensitivity and dynamic range (~30 dB), even if the analog input gain of the oscilloscope

Optics EXPRESS

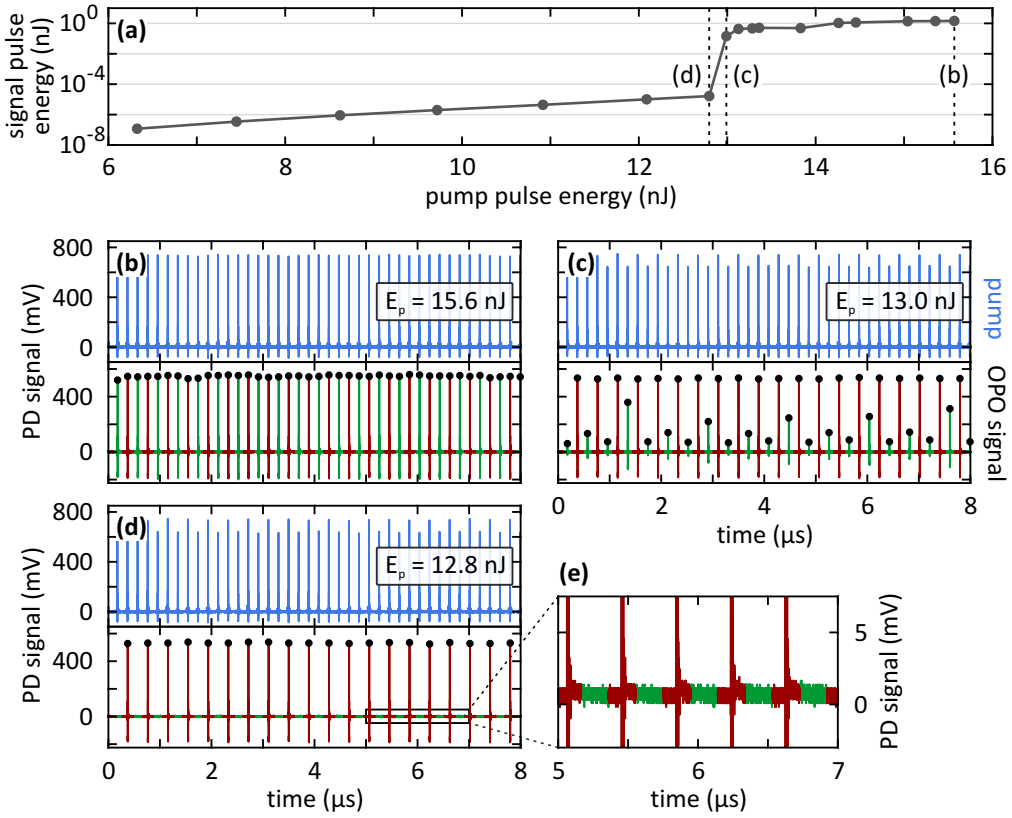

Fig. 3. Contrast ratio investigation to demonstrate the efficiency of the pulse suppression mechanism. **(a)** Signal output pulse energy depending on the pump pulse energy. The FFOPO threshold is between 12.8 and 13.0 nJ below which no signal oscillation occurs, only parametric fluorescence is present. **(b)** The time traces of pump and signal output are shown for three different pump pulse energy levels as indicated in **(a)**. The AOM operates at $m = 8$ and hence, 8 independent signal cycles are launched. Additionally, every 2nd pump pulse is variably attenuated such that the pulse suppression behavior due to the FFOPO threshold can be investigated. The unattenuated pulse train (red) serves as reference for the attenuated pulse train (green). Both pulse trains are equal in panel **(b)** for identical pump energy of 15.6 nJ. Reducing the pump energy near the FFOPO threshold **(c)** leads to decreasing energy in the attenuated pulse trains. Interestingly, the four independent pulse trains also oscillate with different pulse energy. Already slightly below the oscillation threshold **(d)** only the reference pulse train remains, while any intermediate pulses vanish completely. PD: photodiode.

is increased to its maximum. Since a much higher pulse contrast is expected for the FFOPO due to the complete absence of amplified spontaneous emission, we employ a single photon counting module (SPCM). This approach, in principle, allows to scan the entire temporal region of one pulse cycle when combined with a time tagger. In practice, these devices are limited to similar 30 dB contrast ratio due to 0.1% electronical after-pulsing and damage threshold (10^4 photons/pulse), and, suffer from a 25-ns dead time window after a detected event, during which no data can be acquired.

A scanning scheme based on nonlinear optical gating overcomes this dynamic range problem by mapping the signal into a different spectral channel, which thus can be spectrally separated

Optics EXPRESS

from the fundamental and can be detected by the SPCM. This measurement scheme circumvents the limitations of after-pulsing and detector dead time. At gate positions with high nonlinear yield, e.g., the main pulse at time-zero, attenuation of the optical power using neutral density (ND) filters is introduced prior to the SPCM in order to avoid photo damage, and, to extend the dynamic range arbitrarily. Additionally, the temporal resolution is not limited by electronic jitter anymore. It is now given by the gating laser pulse duration, i.e., 450 fs. Thus, the temporal resolution is enhanced by ~3 orders of magnitude.

We realize this scheme with a second-order cross-correlation measurement based on sum-frequency generation (SFG) in a β-barium borate (BBO) crystal (2 mm, $\theta = 23°$) as depicted in Fig. 4(a). The FFOPO signal at 1584 nm and $m = 8$ (5.13 MHz) is being correlated with a portion of the laser oscillator which serves as 450-fs optical gate. Delaying the gating laser with respect to the signal allows scanning of the temporal region between two subsequent signal pulses for any residual optical power at the spectral position of the FFOPO signal. The detection is performed using a single-photon counting module (SPCM) in combination with a time tagging unit (Swabian Instruments, Time Tagger 20). The SFG signal is spectrally separated from all other spectral components before it is sent into the SPCM. The SPCM (Excelitas, SPCM-AQRH-15-FC) exhibits an extremely low dark count rate of only 20 counts/s, and a dead time after a detected event of 25 ns. Thus, at the gating rate of 5.13 MHz the SPCM is fully recovered between possibly occurring events. The FFOPO pump pulse train serves as trigger, such that all signal events are binned into a narrow time range of the acquired histogram. This enhances the signal-to-noise ratio even further as randomly occurring dark counts are equally distributed across all time bins. In combination with accurate ND filtering this method provides an extremely high dynamic range. The sensitivity limit of this method is characterized by replacing the FFOPO signal with a 1550-nm cw laser. As depicted in Fig. 4(b) a cw power level of only 255 pW is still detectable at 100 s integration time per data point. This corresponds to a sensitivity limit of −130 dB with respect to the main signal pulse energy level, and hence, this surpasses the sensitivity in the measurement shown in Fig. 3(e) by 10 orders of magnitude.

A temporal resolution of ~100 fs is achieved by translating the gating pulse with respect to the FFOPO signal pulse using a micrometer stage. For coarse scanning, a 7.3-m (40.95 MHz) folded delay stage is employed. To cover the entire range (5.13 MHz, 59 m), an additional synchronized AOM is used which selects the actual gating pulse from the 40.95 MHz pulse train and thus allows for discrete 7.3-m steps.

Figure 4(c) depicts the optically gated SFG trace which covers one entire FFOPO signal cycle. A signal pulse energy level of 1.2 nJ (6 mW at 5.13 MHz, 1584 nm) corresponds to a total number of photons of $9.3 \cdot 10^9$ per pulse. The respective SFG level at $\Delta\tau = 0$ is set as the reference level to 0 dB. During most of the off-duty cycle the measured SFG level falls below the sensitivity limit, which statistically corresponds to $8.95 \cdot 10^{-4}$ photons per gating window. In this case, the sensitivity limit at −130 dB is assigned to the respective data points as an upper bound level.

The black dots indicate the temporal position of the 7 suppressed pump pulses during one subharmonic cycle ($m = 8$). At the pulse sites adjacent to the main pulse two peaks arise at a level of −111 dB. As indicated in Fig. 1, the limited switching bandwidth of the AOM leads to residual pump pulses which generate parametric fluorescence. Thus, the initial contrast ratio of the AOM of 20:1 is enhanced to $1.3 \cdot 10^{11}$ by the intrinsic threshold characteristics of the FFOPO. All other pump pulse sites do not exhibit any residual optical power above the sensitivity limit.

Leading and trailing pulses at levels between −90 and −60 dB are detected within 1-5 ns temporal separation from the main peak symmetrically to both sides as depicted in Fig. 4(d). These peaks arise from back-reflections of the feedback pulse at optical elements in the FFOPO cavity, even though angled physical contact fiber optics with high return losses are used. The free-space path length between fiber coupler and delay mirror amounts to ~60 cm, which explains the ~2-ns temporal separation between reflected pulse and the main pulse. Further suppression

Optics EXPRESS

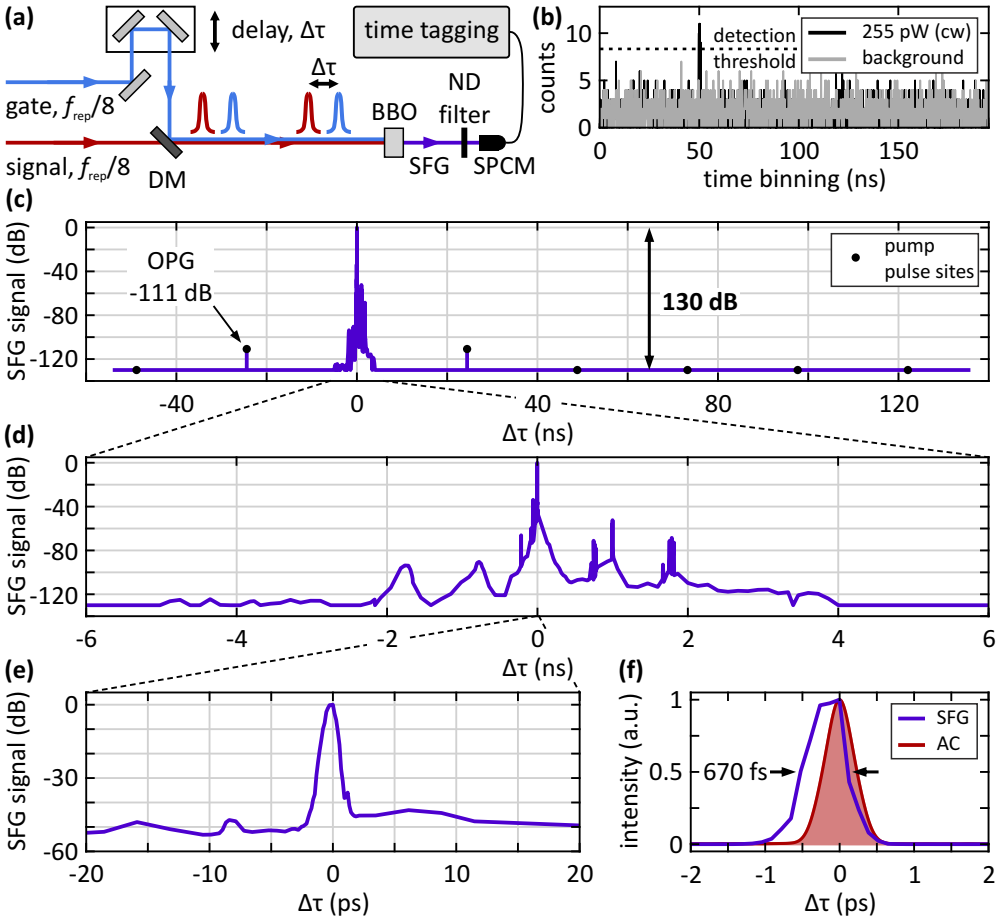

Fig. 4. Temporal pulse contrast ratio of the FFOPO signal output at 1584 nm and $m = 8$ (195.4 ns pulse spacing). **(a)** The SFG cross-correlation between the FFOPO signal output and the pump laser is generated in a BBO crystal and acquired using a SPCM and a time tagging unit. DM: dichroic mirror, BBO: β-barium borate, ND: neutral density, SPCM: single-photon counting module. **(b)** Sensitivity check using a 1550-nm cw-laser instead of the FFOPO signal. The SFG at a cw-power level of 255 pW is still detectable at 10 mW of gating laser power and 100 s integration time. **(c)** SFG cross-correlation trace. At 6 mW of signal power a sensitivity level of −130 dB relative to the maximum signal is reached. The black dots mark the positions of the pump pulse sites. Residual adjacent pump pulses generate parametric fluorescence (OPG) at −111 dB. **(d)** Zoom-in to the ns-timescale. Multiple reflections of the signal at optical elements within the FFOPO cavity cause leading and trailing peaks. **(e)** The ps-timescale reveals the main peak. The background level of −50 dB can be assigned to the dispersively stretched part of the signal feedback which does not experience parametric gain. **(f)** SFG cross-correlation on a linear scale, which exhibits a width of 670 fs at FWHM. Red curve: corresponding auto-correlation (AC) trace of the FFOPO signal, which yields 338 fs pulse duration assuming a Gaussian temporal profile.

of back-reflections would be possible by changing from a linear cavity to a ring-cavity design, where reflections propagating in backward direction do not appear in the output.

Optimally, the gating laser would consist of only one single laser pulse which defines the gating window. However, due to unavoidable reflections at optical elements a number of weak

Optics EXPRESS

ghost pulses accompany the main gating pulse. These ghost pulses undergo the SFG process with the FFOPO signal pulse as well, given that they overlap temporally. Clearly, these ghost pulses cause SFG events with advanced or delayed arrival time at the SPCM, hence they can be temporally separated from the main gating window within the timing histogram. But if this temporal separation falls below the temporal resolution of the electronical gating (~1 ns, corresponding to ~30 cm spatial separation), these undesired events are convoluted into the main gating window and cannot be separated anymore.

Figure 4(e) depicts the ps-range around the main pulse, where pedestals to both sides at a level of −50 dB are observed. The signal feedback propagates through 320 m of SMF, where dispersion causes temporal stretching to ~70 ps at the given signal bandwidth of 12 nm. Only the part which temporally overlaps with the pump pulse experiences a single-pass gain of ~50 dB. In Fig. 4(f) the SFG cross-correlation is depicted on a linear scale together with the auto-correlation (AC) trace of the signal (red curve). Hereby, a pulse duration of 338 fs is extracted assuming a Gaussian temporal profile. A numerical convolution of such a signal pulse with the gate (sech^2, 450 fs) yields a cross-correlation trace with a width of 590 fs. This value is in good agreement with the measured width (670 fs).

Subsequent pulse cleaning of the FFOPO signal output via second-harmonic generation (SHG) would enhance the temporal contrast ratio even further due to its quadratic intensity dependence. Even intense reflections at relative levels of −50 dB would be suppressed down to approximately −100 dB. The same holds for the ps-pedestals at −50 dB around the main pulse. The leading and trailing parametric fluorescence would be suppressed beyond the sensitivity limit.

4. Conclusion

We have demonstrated a wavelength-tunable pulse picking system based on an extended FFOPO cavity, which provides an extremely high (measurement-limited) temporal contrast ratio which exceeds 130 dB. Adjacent pulses are suppressed by 111 dB which offers a superior modulation depth at the Nyquist frequency. The picking performance is independent of the signal output wavelength. Additionally, the tunability extends across the idler wavelength range as well, i.e., 2510–3815 nm for the given signal tuning range. The system has its fundamental pulse repetition rate at the 64^{th} subharmonic of the pump oscillator. Thus, the tunable output pulse train can be varied between 640 kHz and 41 MHz, which enables FLIM measurements with extremely long lifetimes. Effectively, the performance of the pulse picker in the pump beam is enhanced by the subsequent FFOPO system exploiting its nonlinear characteristics.

For an existing synchronously pumped FFOPO system the extended-cavity approach presented in this work offers an easy-to-implement, low-cost upgrade possibility, such that the FFOPO capabilities are extended to variable repetition rates.

Further suppression of reflections can be achieved by changing to a ring cavity, such that backwards-propagating reflections do not appear in the signal output. Additionally, subsequent temporal pulse cleaning via SHG would increase the minimum contrast ratio to ~100 dB. Residual wing pulses caused by parametric fluorescence would be suppressed below the detection limit. Therefore, this system could also be used as front-end system for high-power laser applications which aim for extremely high temporal contrast ratios.

Funding. European Research Council (PoC 3DPRINTEDOPTICS); Carl-Zeiss-Stiftung; Deutsche Forschungsgemeinschaft (GRK 2642); Integrated Quantum Science and Technology (IQST); Baden-Württemberg Stiftung; Bundesministerium für Bildung und Forschung.

Disclosures. The authors declare no conflicts of interest.

Data availability. Data underlying the results presented in this paper are not publicly available at this time but may be obtained from the authors upon reasonable request.

Optics EXPRESS

References

1. S. Lévêque-Fort, D. N. Papadopoulos, S. Forget, F. Balembois, and P. Georges, "Fluorescence lifetime imaging with a low-repetition-rate passively mode-locked diode-pumped Nd:YVO_4 oscillator," Opt. Lett. **30**(2), 168–170 (2005).
2. A. Major, V. Barzda, P. A. E. Piunno, S. Musikhin, and U. J. Krull, "An extended cavity diode-pumped femtosecond Yb:KGW laser for applications in optical DNA sensor technology based on fluorescence lifetime measurements," Opt. Express **14**(12), 5285–5294 (2006).
3. B. R. Masters, P. T. C. So, C. Buehler, N. Barry, J. D. Sutin, W. W. Mantulin, and E. Gratton, "Mitigating thermal mechanical damage potential during two-photon dermal imaging," J. Biomed. Opt. **9**(6), 1265–1270 (2004).
4. P. G. Antal and R. Szipőcs, "Tunable, low-repetition-rate, cost-efficient femtosecond Ti:sapphire laser for nonlinear microscopy," Appl. Phys. B **107**(1), 17–22 (2012).
5. G. Mourou, T. Tajima, and S. V. Bulanov, "Optics in the relativistic regime," Rev. Mod. Phys. **78**(2), 309–371 (2006).
6. J. Itatani, J. Faure, M. Nantel, G. Mourou, and S. Watanabe, "Suppression of the amplified spontaneous emission in chirped-pulse-amplification lasers by clean high-energy seed-pulse injection," Opt. Commun. **148**(1-3), 70–74 (1998).
7. S. Fourmaux, S. Payeur, S. Buffechoux, P. Lassonde, C. St-Pierre, F. Martin, and J. C. Kieffer, "Pedestal cleaning for high laser pulse contrast ratio with a 100 TW class laser system," Opt. Express **19**(9), 8486–8497 (2011).
8. H. Kiriyama, T. Shimomura, H. Sasao, Y. Nakai, M. Tanoue, S. Kondo, S. Kanazawa, A. S. Pirozhkov, M. Mori, Y. Fukuda, M. Nishiuchi, M. Kando, S. V. Bulanov, K. Nagashima, M. Yamagiwa, K. Kondo, A. Sugiyama, P. R. Bolton, T. Tajima, and N. Miyanaga, "Temporal contrast enhancement of petawatt-class laser pulses," Opt. Lett. **37**(16), 3363–3365 (2012).
9. T. J. Yu, S. K. Lee, J. H. Sung, J. W. Yoon, T. M. Jeong, and J. Lee, "Generation of high-contrast, 30 fs, 1.5 PW laser pulses from chirped-pulse amplification Ti:sapphire laser," Opt. Express **20**(10), 10807–10815 (2012).
10. Z. Zhao, K. Mernick, M. Costanzo, and M. Minty, "An ultrafast laser pulse picker technique for high-average-current high-brightness photoinjectors," Nucl. Instrum. Methods Phys. Res., Sect. A **959**, 163586 (2020).
11. Y. Huang, C. Zhang, Y. Xu, D. Li, Y. Leng, R. Li, and Z. Xu, "Ultrashort pulse temporal contrast enhancement based on noncollinear optical-parametric amplification," Opt. Lett. **36**(6), 781–783 (2011).
12. P. Yuan, G. Xie, D. Zhang, H. Zhong, and L. Qian, "High-contrast near-IR short pulses generated by a mid-IR optical parametric chirped-pulse amplifier with frequency doubling," Opt. Lett. **35**(11), 1878–1880 (2010).
13. I. Jovanovic, C. P. J. Barty, C. Haefner, and B. Wattelier, "Optical switching and contrast enhancement in intense laser systems by cascaded optical parametric amplification," Opt. Lett. **31**(6), 787–789 (2006).
14. C. Dorrer, I. A. Begishev, A. V. Okishev, and J. D. Zuegel, "High-contrast optical-parametric amplifier as a front end of high-power laser systems," Opt. Lett. **32**(15), 2143–2145 (2007).
15. H. Kiriyama, M. Mori, Y. Nakai, Y. Yamamoto, M. Tanoue, A. Akutsu, T. Shimomura, S. Kondo, S. Kanazawa, H. Daido, T. Kimura, and N. Miyanaga, "High-energy, high-contrast, multiterawatt laser pulses by optical parametric chirped-pulse amplification," Opt. Lett. **32**(16), 2315–2317 (2007).
16. H. Kiriyama, M. Mori, Y. Nakai, T. Shimomura, M. Tanoue, A. Akutsu, S. Kondo, S. Kanazawa, H. Okada, T. Motomura, H. Daido, T. Kimura, and T. Tajima, "High-contrast, high-intensity laser pulse generation using a nonlinear preamplifier in a Ti:sapphire laser system," Opt. Lett. **33**(7), 645–647 (2008).
17. R. C. Shah, R. P. Johnson, T. Shimada, K. A. Flippo, J. C. Fernandez, and B. M. Hegelich, "High-temporal contrast using low-gain optical parametric amplification," Opt. Lett. **34**(15), 2273–2275 (2009).
18. I. Musgrave, W. Shaikh, M. Galimberti, A. Boyle, C. Hernandez-Gomez, K. Lancaster, and R. Heathcote, "Picosecond optical parametric chirped pulse amplifier as a preamplifier to generate high-energy seed pulses for contrast enhancement," Appl. Opt. **49**(33), 6558–6562 (2010).
19. E. Cunningham, E. Galtier, G. Dyer, J. Robinson, and A. Fry, "Pulse contrast enhancement via non-collinear sum-frequency generation with the signal and idler of an optical parametric amplifier," Appl. Phys. Lett. **114**(22), 221106 (2019).
20. A. Jullien, O. Albert, F. Burgy, G. Hamoniaux, J.-P. Rousseau, J.-P. Chambaret, F. Augé-Rochereau, G. Chériaux, J. Etchepare, N. Minkovski, and S. M. Saltiel, "10^{-10} temporal contrast for femtosecond ultraintense lasers by cross-polarized wave generation," Opt. Lett. **30**(8), 920–922 (2005).
21. A. Cotel, A. Jullien, N. Forget, O. Albert, G. Chériaux, and C. Le Blanc, "Nonlinear temporal pulse cleaning of a 1-μm optical parametric chirped-pulse amplification system," Appl. Phys. B **83**(1), 7–10 (2006).
22. H. Liebetrau, M. Hornung, A. Seidel, M. Hellwing, A. Kessler, S. Keppler, F. Schorcht, J. Hein, and M. C. Kaluza, "Ultra-high contrast frontend for high peak power fs-lasers at 1030 nm," Opt. Express **22**(20), 24776–24786 (2014).
23. J.-L. Tapié and G. Mourou, "Shaping of clean, femtosecond pulses at 1.053 μm for chirped-pulse amplification," Opt. Lett. **17**(2), 136–138 (1992).
24. Y. Beaudoin, C. Y. Chien, J. S. Coe, J. L. Tapié, and G. Mourou, "Ultrahigh-contrast Ti:sapphire/Nd:glass terawatt laser system," Opt. Lett. **17**(12), 865–867 (1992).
25. D. Homoelle, A. L. Gaeta, V. Yanovsky, and G. Mourou, "Pulse contrast enhancement of high-energy pulses by use of a gas-filled hollow waveguide," Opt. Lett. **27**(18), 1646–1648 (2002).
26. H. C. Kapteyn, M. M. Murnane, A. Szoke, and R. W. Falcone, "Prepulse energy suppression for high-energy ultrashort pulses using self-induced plasma shuttering," Opt. Lett. **16**(7), 490–492 (1991).

Optics EXPRESS

27. A. Lévy, T. Ceccotti, P. D'Oliveira, F. Réau, M. Perdrix, F. Quéré, P. Monot, M. Bougeard, H. Lagadec, P. Martin, J.-P. Geindre, and P. Audebert, "Double plasma mirror for ultrahigh temporal contrast ultraintense laser pulses," Opt. Lett. **32**(3), 310–312 (2007).
28. V. A. Schanz, C. Brabetz, D. J. Posor, D. Reemts, M. Roth, and V. Bagnoud, "High dynamic range, large temporal domain laser pulse measurement," Appl. Phys. B **125**(4), 61 (2019).
29. A. Steinmann, B. Metzger, R. Hegenbarth, and H. Giessen, "Compact 7.4 W femtosecond oscillator for white-light generation and nonlinear microscopy," *CLEO: 2011 - Laser Science to Photonic Applications*, Baltimore, MD, 2011, pp. 1–2.
30. T. Steinle, F. Mörz, A. Steinmann, and H. Giessen, "Ultra-stable high average power femtosecond laser system tunable from 1.33 to 20 µm," Opt. Lett. **41**(21), 4863–4866 (2016).
31. F. Mörz, T. Steinle, A. Steinmann, and H. Giessen, "Multi-Watt femtosecond optical parametric master oscillator power amplifier at 43 MHz," Opt. Express **23**(18), 23960–23967 (2015).